How to Cite: Lahmar, N., Djehiche, M., & Bachiri, M. (2024). Removal of E110 from Aqueous Solution Using Heat-Activated Persulfate. *Eurasian Journal of Chemistry, 29, 4(116), 22–34.* https://doi.org/10.31489/2959-0663/4-24-6

PHYSICAL AND ANALYTICAL CHEMISTRY

Article

Received: 2 July 2024 | Revised: 21 October 2024 |
Accepted: 5 November 2024 | Published online: 23 November 2024

UDC 542.943+628.161

https://doi.org/10.31489/2959-0663/4-24-6

Nedjma Lahmar, Mokhtar Djehiche*, Marwa Bachiri

Inorganic Materials Laboratory, University of M'sila, M'sila, Algeria
*(*Corresponding author's e-mail: mokhtar.djehiche@univ-msila.dz)*

Removal of E110 from Aqueous Solution Using Heat-Activated Persulfate

This paper presents an investigation into the efficiency of heat-activated persulfate (PS) in decolorizing E110 with a focus on the influence of several parameters. The decolorization efficiency was observed to increase with rising PS concentration (no linear correlation was identified), Cl^-, temperature, and time. However it was noted to decrease with rising initial dye concentration, pH, ion radius and NO_2^-. The rest of the water matrix components (CO_3^{2-}, HPO_4^{2-}, HCO_3^-, and NO_3^-) did not significantly impact on the degradation of E110 at 10^{-3} M. Among the metal ions used (Fe^{2+}, Ni^{2+}, Co^{2+}, Cu^{2+}, and Ag^+), iron and silver ions exhibited the greatest efficacy in activating PS through catalysis. A direct reaction between E110 and PS was not observed, as is the case with some anionic dyes, instead its degradation occurs via sulfate radicals (SRs) and other secondary mechanisms. The results of biological and chemical oxygen demand measurements indicate that E110 is not biodegradable. The kinetic activation parameters (E_a, $\Delta H^{\neq}$, $\Delta S^{\neq}$, $\Delta G^{\neq}$) were calculated using Arrhenius and Eyring's equations. The results obtained were as follows: 155.4 kJ mol^{-1}, 152.7 kJ mol^{-1}, 0.14 kJ K^{-1}, 108.5 kJ mol^{-1}. Finally, a preliminary mechanism for the degradation of E110 by SR has been proposed, in which the destruction of aromatic ring structures accompanies the discoloration of E110.

Keywords: E110, persulfate, sulfate radical, dye decolorization, kinetic activation parameters, mechanism, heat-activated persulfate, aqueous solution, biodegradable.

Introduction

Many chemical industries use dyes, that produce toxic and carcinogenic wastewater, contaminating water and polluting the environment. The removal of color from waste is often more important than the removal of other colorless and organic substances because the presence of a small amount of dye (below 1 ppm) is easily visible and has a significant impact on the water environment [1]. A color additive is a substance that is added to food, drink, or other products to change their color. It can be a dye, pigment, or any other substance that reacts with another substance to produce color. Color additives are used for a variety of purposes, including compensating for color loss, enhancing natural colors to make them more appealing, adding color to initially colorless food products, and facilitating product identification, especially in the case of pharmaceuticals [2]. Synthetic colorants are preferred over natural colorants because they are less expensive, more stable, and more resistant to light, oxygen, and pH [3]. Recently, more attention has been paid to their toxicity, especially azo dyes [4]. Azo dyes represent the majority of dyes used in many industries because the azo bond (–N=N–) promotes the delocalization of π electrons, resulting in absorption at visible spectrum wavelengths [5]. Azo dyes are highly toxic due to the mutagenic nitro group, and they decompose to produce toxic products such as 1,4-phenylenediamine and o-tolidine [6]. Certain microorganisms can degrade azo dyes, yielding toxic, mutagenic, and carcinogenic intermediates [7]. E110, an azo dye, is a well-known synthetic food dye found in Kellogg's, hot fudge sundaes, tarts, soft drinks, and candies [8, 9]. This includes applications other than food, such as pharmaceutical, cosmetic, and textile products [10]. E110 is safe at a daily

dose of less than 2.5 mg/kg [2]. At high concentrations, it exhibits xenoestrogenic activity [11]. E110, among other dyes, is the type of food dye most commonly associated with human carcinogens [12].

PS (peroxydisulfate, $S_2O_8^{2-}$), a compound used in situ chemical oxidation (ISCO) technology, is a chemical oxidant for soil and groundwater decontamination [13]. This process treats a wide range of impurities using direct electron transfer or free radical processes, including halogenated olefins, BTEXs (benzene, toluene, ethylbenzene, and xylenes), perfluorinated chemicals, phenols, pharmaceuticals, inorganics, and pesticides [14]. The radical process generates SRs ($SO_4^{\cdot-}$) by activating PS (R1) with heat [15, 16], transition metals [17, 18], ultraviolet (UV) light [19] and other means [20–22]. Thermal treatment is expensive, which limits its use in pollutant removal. Despite the high cost of thermal treatment, which limits its use in pollutant removal, the use of solar thermal energy [23, 24] simplifies the use of heat to activate PSs. This approach uses solar energy as a heat source, which increases the efficiency of the PS activation process. PS ions decompose thermally (k_2 varies from 5.85×10^{-8} s^{-1} at 30 °C to 1×10^{-4} s^{-1} at 80 °C [13, 14, 25, 26]) to form two SRs (Eq. 2), which react with PS anions (Eq. 3), water (Eq. 4), self-reaction (Eq. 5) and organic compounds (Eq. 6):

$$S_2O_8^{2-} + \text{Activator} \rightarrow 2\ SO_4^{\cdot-} \quad (1)$$

$$S_2O_8^{2-} + \text{Heat} \rightarrow 2\ SO_4^{\cdot-} \quad (2)$$

$$S_2O_8^{2-} + SO_4^{\cdot-} \rightarrow S_2O_8^{\cdot-} + SO_4^{2-} \quad (3)$$

$$SO_4^{\cdot-} + H_2O \rightarrow OH\cdot + H^+ + SO_4^{2-} \quad (4)$$

$$SO_4^{\cdot-} + SO_4^{\cdot-} \rightarrow S_2O_8^{2-} \quad (5)$$

$$SO_4^{\cdot-} + \text{E110} \rightarrow \text{Product} \quad (6)$$

According to Eq. 7, the SR can react with elements present in the water matrix (X^-) such as Cl^-, CO_3^{2-}, HPO_4^{2-}, HCO_3^-, NO_2^- and NO_3^- [27, 28]. This results in the formation of a radical ($X\cdot$), which then reacts with organic compounds to decolorize them. However, the reaction between the produced radicals and non-target chemical species, whether natural or artificial, reduces reaction efficiency, resulting in a significant limitation [29].

$$SO_4^{\cdot-} + X^- \rightarrow X\cdot + SO_4^{2-} \quad (7)$$

PS can be activated by transition metals, including Fe^{2+}, Co^{2+}, Ni^{2+}, Cu^{2+}, and Ag^+, resulting in the formation of SRs as shown in Eq. 23, where Mn^{n+} represents typical metal ions [17, 18, 30]:

$$S_2O_8^{2-} + Mn^{n+} \rightarrow Mn^{n+} + SO_4^{\cdot-} + SO_4^{2-} \quad (8)$$

The use of metal ions poses practical problems, particularly in terms of recycling and secondary pollution. However, iron ions and their oxides have been extensively studied, due to their environmentally-friendly, non-toxic and low-cost characteristics [31].

pH has a significant impact on dyes' chemical structure, stability, and ability to absorb light. Thus, pH is an important consideration when designing and maintaining in-situ chemical oxidation systems [32, 33]. Previous studies have investigated the decolorization of E110 through biological processes [34], adsorption [35], UV/H_2O_2, ultrasound [36], photocatalytic [1], and Fenton. However, the use of the activated PS process to degrade E110 has not been extensively researched. Although the activated PS process has been used to decolorize a variety of substances, including Acid blue 92, naphthalene, methylene blue, Ponceau 6R dye, sulfamethazine, trichloroethane, carbamazepine, propylparaben, polycyclic aromatic hydrocarbons, and metronidazole [37], its application to E110 is novel.

Thus, the study aims to assess the efficacy of heat-activated PS for E110 decolorization in aqueous solution. The study investigates the effects of activation temperature, PS concentration, time, water matrix, transition metals, and dye concentrations. It also investigates decolorization kinetics and thermodynamic properties such as Gibbs free energy, activation energy, and reaction entropies. Based on the results and the literature, we propose a mechanism for the degradation of E110 dye.

Experimental

This study utilized the following chemicals: E110 ($C_{16}H_{10}N_2Na_2O_7S_2$, 90 % Sigma–Aldrich), potassium persulfate ($K_2S_2O_8$, 99 % Merck), sulfuric acid (H_2SO_4, 97 % Honeywell), hydrochloric acid (HCl, 37 % Honeywell), sodium hydroxide (NaOH, 99 % Biochem Chemopharma), sulfuric acid heptahydrate ($FeSO_4\cdot7H_2O$, 99 % Sigma–Aldrich), sulfuric acid ($CuSO_4$, 97 % Biochem Chemopharma), silver nitrate

($AgNO_3$, 99 % Biochem Chemopharma), sodium chloride (NaCl, 99.5 % Honeywell), potassium chloride (KCl, 99 % Sigma–Aldrich), and sodium sulfate (Na_2SO_4, 99 % Sigma–Aldrich), sodium bicarbonate ($NaHCO_3$,99.7 % Honeywell), sodium phosphate (Na_2HPO_4, 98 % Panreac), sodium nitrite ($NaNO_2$, 98 % Fluka), and sodium nitrate ($NaNO_3$, 99.5 % Biochem Chemopharma). Distilled water was used to prepare the study solutions. After dissolving the required amount of PS for the reaction medium in 5 ml of distilled water, the mixture was added to a beaker containing 200 ml of E110 solution and heated to the desired temperature with a thermostat. A Metrohm Model 781 pH/Ion meter was used to continuously monitor pH 3, which serves as the baseline for all tests. The decolorization process of the dye solutions was investigated using a 2401 PC UV spectrophotometer (Shimadzu, optical path = 1 cm), which measured dye absorbance at 480 nm. Chemical oxygen demand (COD) was measured using the ISO 6060 method, while biological oxygen demand (BOD5) is measured with the BOD 901 meter (made in Europe).

Results and Discussion

Effect of Initial PS and E110 Concentration

Figure 1 (top) depicts the effect of initial PS concentration on E110 elimination effectiveness. The decolorization process was completed in less than 90 minutes with PS concentrations of 7.4, 3.7, and 1.84 mM, but it took more than 200 minutes with concentrations of 0.92 and 0.18 mM. This indicates that elevated PS concentrations result in the formation of a greater number of SRs, thereby accelerating the oxidation of E110 [16, 37]. This relationship is not linear due to the nonlinear plot of E110 half-life values ($t_{1/2}$) as a function of initial PS concentration (Figure 1 bottom) is nonlinear, and its increase becomes meaningless at concentrations above 3.7 mM. This result is explained by an excess of PS in the solution, which slows the decolorization of E110. An excess of PS concentration can cause the following processes which slow down the decolorization mechanism [38]: (a) excess SO_4 radical recombination and annihilation (Eq. 5), (b) SR consumption with excess PS (Eq. 3), and (c) the occurrence of an unproductive PS decomposition reaction (with no generation of SR).

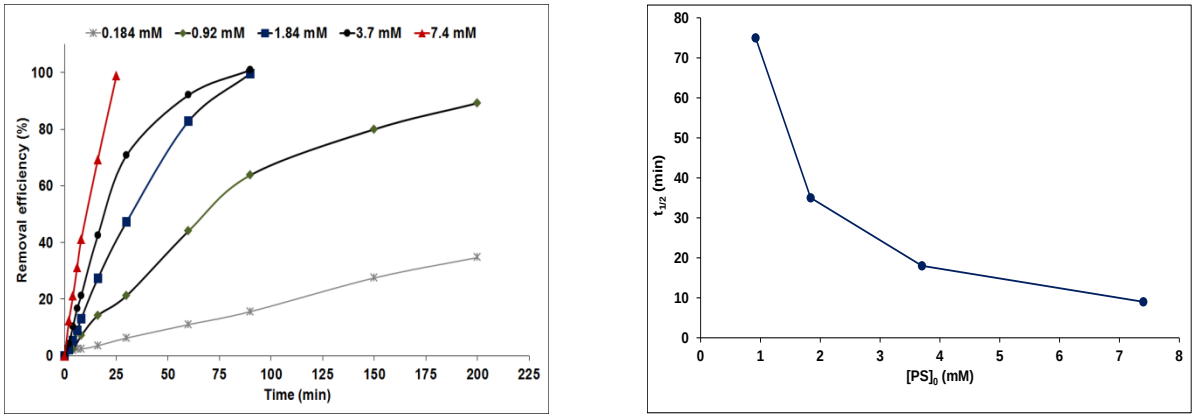

Figure 1. Evolution of E110 decolorization. Top: time dependence of E110 at different initial PS concentrations. Bottom: Plot of E110 half-life time ($t_{1/2}$) values as a function of initial PS concentration. Initial conditions: $[E110]_0$ = 0.66 mM, pH = 3 and T = 60 °C. Removal efficiency (%) = $(([E110]_0 - [E110]_t)/[E110]_0)*100$, where $[E110]_0$ is the concentration at time 0 and $[E110]_t$ is the concentration at time *t*

On the other hand, different initial E110 concentrations of 0.22 mM, 0.66 mM, 1.33 mM, and 1.99 mM were investigated to determine the effect of the initial E110 concentration on elimination. The initial PS concentration was 3.7 mM, and the temperature remained constant at 60 °C. Figure 2 depicts a decrease in PS decolorization efficiency as the concentration of E110 increases. These results can be explained by the dye's high concentration, which consumes free radicals and thus reduces bleaching efficacy [27]. These results are consistent with previous research on the decolorization of other dyes by PS [39, 40]. In the remainder of this study, the PS concentration is limited to 3.7 mM for 0.66 mM of E110, as a higher concentration will not contribute to further improvement in E110 decolorization.

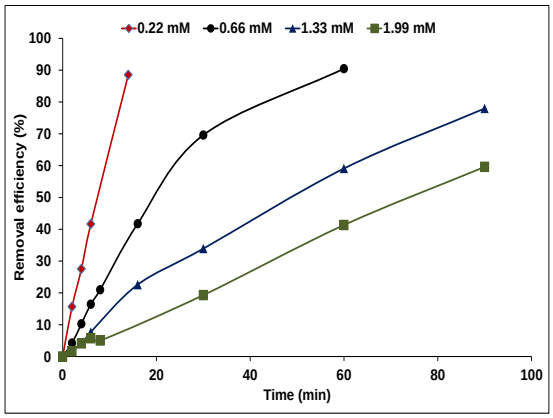

Figure 2. Time dependence of E110 removal efficiency at different initial E110 concentrations (initial conditions: $[PS]_0$ = 3.7 mM, pH = 3 and T = 60 °C)

Kinetic Study

The first- and second-order plots against time of the experimental points ([PS]/[E110] = 0.27 and 11.2), Figures 3*a* and 3*b* indicate that the reaction follows pseudo-first-order kinetics with an R^2 value (>0.99). This is in contrast to pseudo-second-order kinetics which excibits an R^2 value (<0.99). It is well known that second-order reactions can exhibit first-order kinetics in a quasi-steady state [30, 41, 42], where one of the two reactants is in excess of the other. However, despite the low [PS]/[E110] ratios (0.27 and 11.2), the experiments demonstrate first-order kinetics. This is due to the presence of SRs, which are, by definition, in quasi-stationary concentration [30, 41, 42], implying that the variation in SR concentration is zero ($\Delta[SO_4^{\bullet -}] = 0$). A number of studies on the decolorization of various dyes, conducted under conditions similar to ours, have reported SR concentrations of around 10^{-12} M [41, 43, 44], which are significantly lower than the concentration of E110. Thus, the decolorization of E110 can be thought to follow first-order kinetics, as described in Eq. 9.

$$-\frac{d[\mathrm{E110}]}{dt} = k_6\left[SO_4^{\bullet -}\right][\mathrm{E110}] = k_{obs}[\mathrm{E110}], \tag{9}$$

where k_6 represents the second-order rate constant reaction of E110 with SR (Eq. 6), and k_{obs} represents the observed rate constant for E110 decolorization.

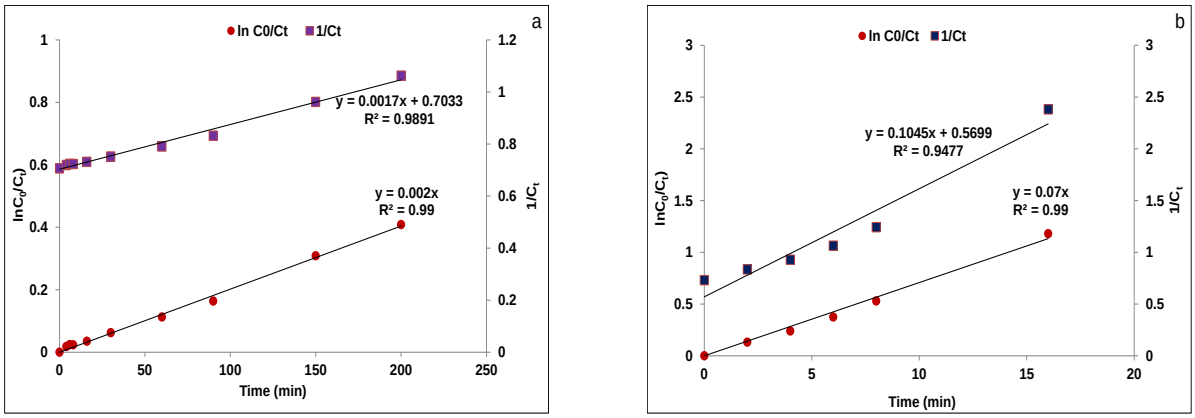

Figure 3. Plots of first and second-order E110 decolorization at [PS]/[E110] ratios of a) 0.27 and b) 11.2. (Initial conditions: $[E110]_0$ = 0.66 mM, pH = 3 and T = 60 °C)

We used a numerical simulation model developed in our previous work [45, 46] to investigate the reaction between E110 and the dominant SRs (Eq. 6) at pH 3. With the exception of k_6 (Table 1), all rate constants were known; therefore, the latter was adjusted to ensure that the model matched experimental data (Fig. 4).

Table 1

Rate constants for E110 degradation

Chemical reactions	Rate constants				Units	References
	25 °C	40 °C	50 °C	60 °C		
Equation (2)	0.25	3.36	19.4	59.4	$\times 10^{-7}$ [s^{-1}]	[47]
Equation (3)	6.1	6.1	6.1	6.1	$\times 10^{5}$ [M^{-1} s^{-1}]	[48]
Equation (4)*	6.2	7.4	8.3	9.2	$\times 10^{2}$ [s^{-1}]	[43]
Equation (5)	4.8	4.8	4.8	4.8	$\times 10^{8}$ [M^{-1} s^{-1}]	[49]
Note: *The indicated rate constant is equal to $k_4 \times [H_2O]$.						

The k_6 values used for the fit (5×10^{10} M^{-1} s^{-1}) are significantly higher than those reported for other dyes in the literature (< 1×10^{10} M^{-1} s^{-1}) [50]. This finding suggests that E110 is degraded not only by SRs but also through other mechanisms. One reason for this observation is the direct reaction between the E110 dye and the PS ion, which has also been observed at ambient temperature with many other anionic and cationic dyes, including Orange II and Rhodamine B [51, 52]. After 90 minutes of monitoring the absorbance of the E110 dye in the PS/E110 reaction mixture at 25 °C, it can be noted that there was no direct reaction between PS and E110 (Fig. 4).

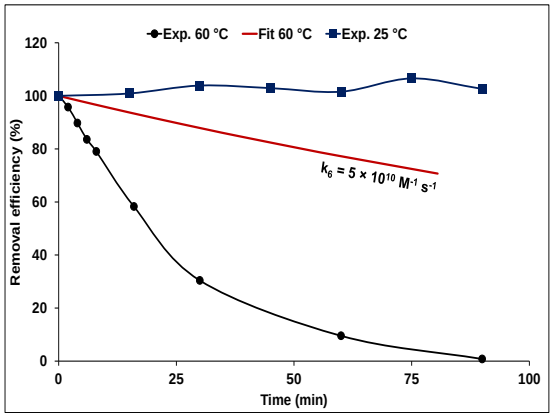

Figure 4. Time dependence of E110 removal efficiency
(initial conditions: $[E110]_0$ = 0.66 mM, $[PS]_0$ = 3.7 mM, pH = 3)

Influence of Water Matrix on E110 Removal

Fixed quantities (10^{-3} M) of chloride, carbonate, nitrate, nitrite, and hydrogenphosphate ions were added to the E110/PS solution to determine the impact of these ions on the decolorization. Figure 5 depicts the evolution of removal efficiency over time. The chloride ion has the highest efficiency, while the nitrite ion has the lowest when compared to the control. According to previous studies [27, 28], chloride ions, through the chlorine radical ($Cl^{\bullet}$), are more effective than other elements found in water, such HPO_4^{2-}, CO_3^{2-} and NO_3^-, for the decolorization of dyes. The low efficiency of nitrite has been attributed to its ability to scavenge SR, resulting in the generation of the nitrogen dioxide radical ($NO_2^{\bullet}$), which contributes to the formation of nitroaromatic by-products [53, 54]. The other salts have varying degrees of effectiveness compared to the control solution.

Figure 6 shows that the removal of E110 in the presence of monovalent cations with a common anion (Cl^-) proceeds in the following order: KCl > NaCl > HCl. Despite having the same ionic strength of 0.0005 M, the monocations have different effects on E110 decolorization.

This result is proportional to the ranking of the three cations according to their ionic radius ($K^+ > Na^+ > H^+$ [55]), whereby a larger radius is associated with a faster degradation kinetic. Despite the limited data on this phenomenon, it has been shown that each cation exerts a distinct influence on the degradation of the pollutant by affecting the activation energy of persulfate decomposition [56, 57].

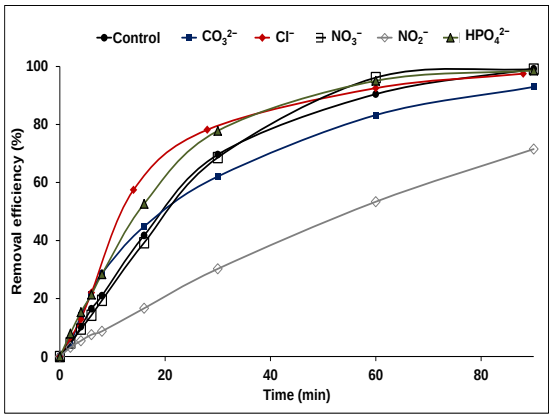

Figure 5. Time dependence of E110 removal efficiency at different initial salt concentrations (initial conditions: $[E110]_0$ = 0.66 mM, $[PS]_0$ = 3.7 mM, $[Salts]_0$ = 1 mM, pH = 3 and T = 60 °C)

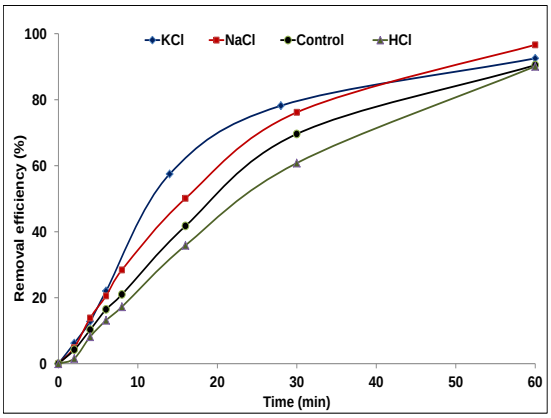

Figure 6. Effects of monovalent cations on the removal of E110 (initial conditions: $[E110]_0$ = 0.66 mM, $[PS]_0$ = 3.7 mM, $[Salts]_0$ = 1 mM, pH = 3 and T = 60 °C)

Effect of Transition Metals

To study the effect of specific transition metals on PS activation, we chose four types of ions (Fe^{2+}, Ni^{2+}, Cu^{2+}, Ag^+) and investigated their influence on E110 decolorization (Fig. 7). The initial concentrations of these four ions were held constant at 10^{-3} M, with 0.66 mM for the E110 and 3.7 mM for the PS. The decolorization of E110 occurred rapidly when iron was added, less rapidly when silver was added, and more slowly in the presence of copper, nickel, and cobalt. This observation is consistent with the results of several studies, in which silver and iron were found to be one of the most effective routes for generating sulfate radicals from persulfate [58, 59]. The difference in catalytic capacity cannot be attributed solely to the redox potential of each metal, but also to factors such as charge, ionic radius, and electronic structure [60].

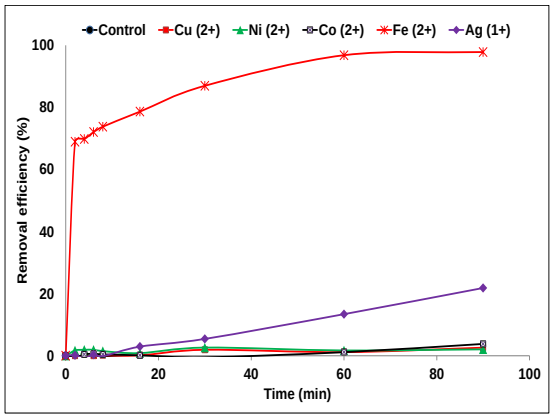

Figure 7. Time dependence of E110 removal efficiency at different initial transition metal concentrations (initial conditions: $[E110]_0$ = 0.66 mM, $[PS]_0$ = 3.7 mM, $[Mn^{n+}]_0$ = 1 mM, pH = 3 and T = 25 °C)

Effect of pH on E110 removal

Figure 8 shows the decolorization of E110 (0.66 mM) by PS (0.18 mM) at 60 °C and different pH values. In order to offset the decline in solution pH resulting from the generation of the H^+ proton (Eq. 4) and the addition of PS, the initial PS concentration was decreased in comparison to the previous experiments. The efficiency of dye elimination efficiency was observed to decline as the pH of the solution increased. This result has been reported in numerous studies and is explained by a decrease in the concentration of SRs, which react with hydroxide ions [61–64]. Similar elimination efficiencies were observed at pH levels 3 and 4, as well as 9 and 11 [65]. This result can be explained by the use of low PS concentrations, which resulted in similar elimination efficiencies across pH values. At pH 2, E110 has higher removal efficiency than at other pH values due to the greater production of SRs (Eq. 10) resulting from acid catalists [66]:

$$S_2O_8^{2-} + H^+ \rightarrow SO_4^{\cdot -} + SO_4^{2-} + H^+ \quad (10)$$

On the other hand, at pH 12, E110 elimination efficiency improves when compared to alkaline pH values 9 and 11. This finding is explained by the formation of hydroxyl radicals (Eq. 11), which becomes more important as pH increases [67, 68], resulting in more hydroxyl radicals that contribute to dye decolorization.

$$SO_4\cdot^- + OH^- \rightarrow OH\cdot + SO_4^{2-} \quad (11)$$

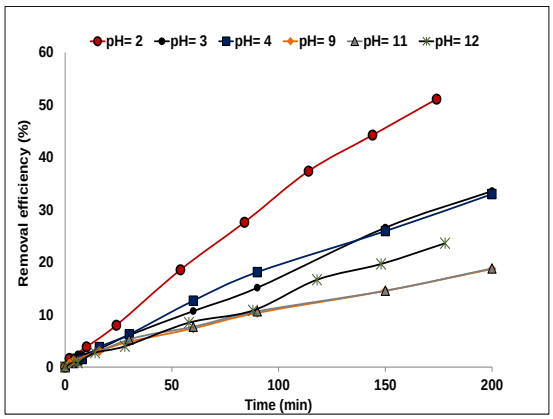

Figure 8. Time dependence of E110 removal efficiency at different pH values (initial conditions: $[E110]_0$ = 0.66 mM, $[PS]_0$ = 3.7 mM and T = 60 °C)

Biochemical and Chemical Oxygen Demand

To determine the biodegradability of the dye, we need to measure both the Chemical Oxygen Demand (COD) and the Biochemical Oxygen Demand over five days (BOD). The BOD5/COD ratio indicates whether or not the dye is biodegradable. COD and BOD5 were measured in a 300 mg/L E110 solution at pH 3 and 20 °C. We measured 2 and 1800 mg/L of BOD5 and COD, respectively. As previously stated [69], the chemical oxygen demand for contaminants from the food and beverage industry pollutants can range from 700 to 3000 mg/L. Thus, the E110 solution has a five-day biochemical oxygen demand/chemical oxygen demand (BOD5/COD) ratio of 0.001, indicating that it is a non-biodegradable dye. Several studies on azo dyes consider them to be non-biodegradable colorants [70, 71].

Effect of Temperature

The effect of temperature on E110 decolorization was investigated at four different heating temperatures (40, 50, 60, and 70 °C). Throughout the experiments, we kept the initial concentration of E110 at 0.66 mM, PS at 3.7 mM, and pH at 3 (Fig. 9). The increased temperature had a positive effect on E110 decolorization. Indeed, elevated temperatures cause the O–O bond in PS to cleave, resulting in the formation of SR and thus accelerating the decomposition of E110 [72, 73].

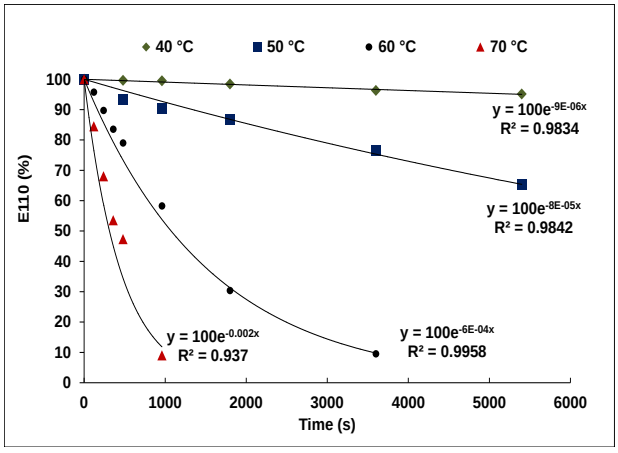

Figure 9. Time dependence of E110 removal efficiency at different temperatures (initial conditions: $[E110]_0$ = 0.66 mM, $[PS]_0$ = 3.7 mM, pH = 3 and T = 60 °C)

The activation parameters associated with decolorization are calculated using Arrhenius and Eyring's equations (Eqs. 12, 13, and 14) [39, 52] and by plotting $\ln(K_{obs})$ and $\ln(K_{obs}/T)$ vs. $1/T$, respectively (Fig. 10):

$$SO_4^{\cdot -} + OH^- \rightarrow OH^{\cdot} + SO_4^{2-} \quad (11)$$

where A is the frequency factor, E_a is the activation energy (kJ·mol^{-1}), R is the gas constant (J·mol^{-1}·K^{-1}), and T is the absolute temperature (K).

$$\ln\left(\frac{k_{obs}}{T}\right) = \left(\ln\left(\frac{k_B}{h}\right) + \frac{\Delta S^{\neq}}{R}\right) - \frac{\Delta H^{\neq}}{RT} \quad (13)$$

where, k_B is the Boltzmann constant (1.38×10^{-23} J K^{-1}), h is Planck's constant (6.626×10^{-34} J s), and $\Delta H^{\neq}$ and $\Delta S^{\neq}$ are the enthalpy and entropy of activation, respectively.

The free activation energy ($\Delta G^{\neq}_{298}$) was determined using Eq. 14 at a T value equal to 298.15 K:

$$\Delta G^{\neq}_{298} = \Delta H^{\neq} - T\Delta S^{\neq} \quad (14)$$

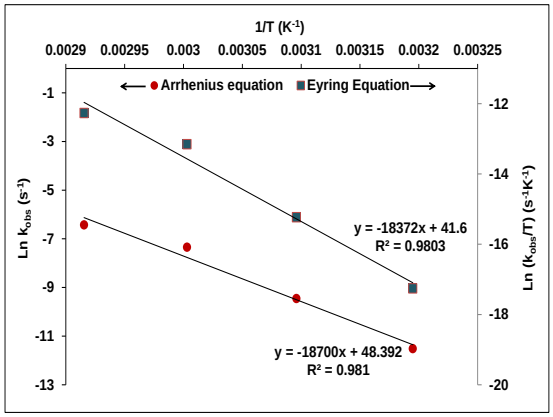

Figure 10. Arrhenius and Eyring Eq. plots for E110 decolorization
($[E110]_0$ = 0.66 mM, $[PS]_0$ = 3.7 mM, pH = 3 and T = 40, 50, 60 and 70 °C)

The positive values for activation energy, enthalpy, entropy, and free energy (Table 2) indicate that the oxidation process requires a minimal amount of energy. Furthermore, it is described as endothermic, with little variation in the three-dimensional arrangement of the molecule's transition state [74].

Table 2

Activation thermodynamic parameters of the decolorization E110 by PS ($[E110]_0$ = 0.66 mM, $[PS]_0$ = 3.7 mM, pH = 3 and T = 40, 50, 60 and 70 °C)

E_a (kJ mol^{-1})	$\Delta H^{\neq}$ (kJ mol^{-1})	$\Delta S^{\neq}$ (kJ K^{-1})	$\Delta G^{\neq}_{298}$ (kJ mol^{-1})
155.4	152.7	0.14	108.5

Orange G has an apparent activation energy of 92 kJ mol^{-1} [75], a structure similar to E110, and a concentration six times lower. It is important to note that the apparent activation parameters are determined by the dyes' initial concentrations and structures of the dyes [37, 74]. The oxidation of E110 by hydrogen peroxide in an alkaline medium required activation energy, enthalpy, entropy, and free energy of 51 kJ mol^{-1}, 54 kJ mol^{-1}, +0.14 kJ K^{-1}, 10.3 kJ mol^{-1}, respectively [74].

UV-Visible Spectrum Analysis

The UV-visible spectra in Figure 11 show the decolorization of E110 using heated PS at 60 °C and pH 3. The characteristic absorption peak at 478 nm corresponds to E110's azo group [N=N], which is responsible for its color. In contrast, the peaks at 269 and 310 nm in the ultraviolet region are attributed to the phenyl and naphthyl groups, respectively [64].

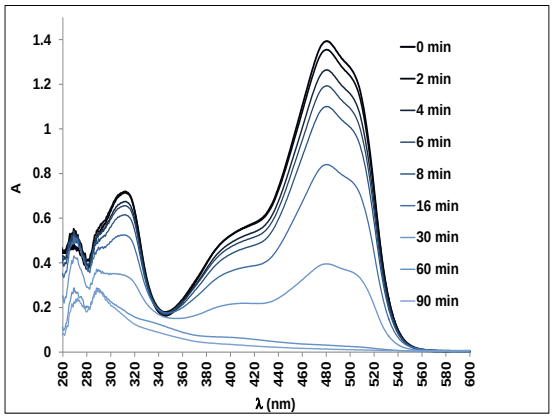

Figure 11. UV-VIS spectra of E110 solution during the decolorization by PS ($[E110]_0$ = 0.66 mM, $[PS]_0$ = 3.7 mM, pH = 3 and T = 60 °C)

During the reaction, the two distinct absorption peaks at 310 nm and 478 nm decreased significantly and nearly vanished after 90 minutes. This observation indicates the complete destruction of the chromophore and conjugated π system. In contrast, the peaks at 259 and 289 nm gradually decrease, indicating that the aromatic rings were still present and frequently were more difficult to oxidize than the azo structure [76, 77]. In general, the action of SRs on organic compounds causes hydroxylation. SRs react with water to form hydroxyl radicals (Eq. 4), which can then interact with aromatic rings to form hydroxyl adducts [48, 78]. SRs could also attack the aromatic ring directly, forming hydroxyl adducts [48, 79], or both processes may occur concurrently [80]. Based on the present results and the existing literature [48, 50, 74, 74, 78], E110 oxidation can occur via two mechanisms: symmetrical azo bond cleavage and asymmetrical azo bond cleavage (Fig. 12).

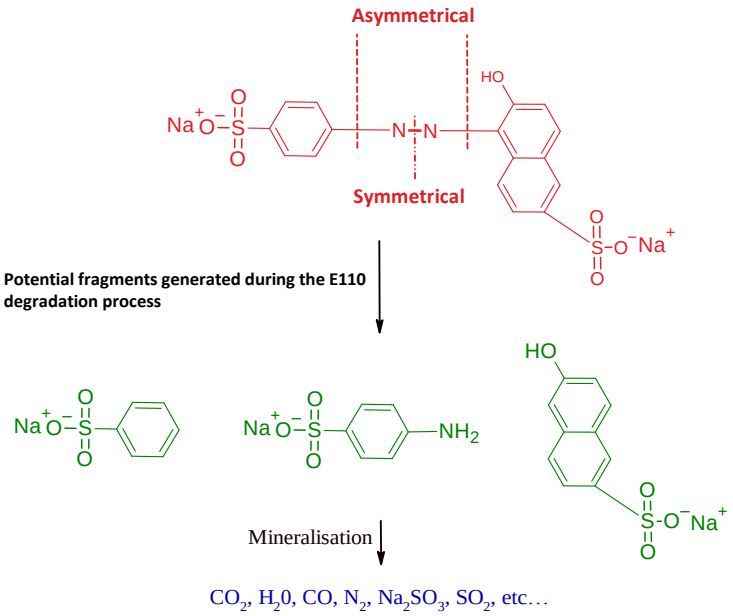

Figure 12. Possible route to the fragments of the E110 dye

Conclusion

This study focused on investigating the process of decolorizing E110 in an aqueous solution using thermally activated peroxydisulfate at a pH level of 3. The findings demonstrated that the effectiveness of E110 decolorization was enhanced by heating and by increasing the initial PS concentration. Conversely, an increase in the initial E110 concentration while the PS concentrations remain constant, will result in a reduction in E110 removal. The introduction of Cl^-, CO_3^{2-}, HPO_4^{2-}, HCO_3^-, NO_2^- or NO_3^- into the dye solutions

typically results in different impacts on the rates of decolorization. The extent of these effects varies depending on the specific salt utilized.

The chlorine ion exhibited the highest level of effectiveness among the tested ions, whereas the nitrite ion demonstrated the lowest level of effectiveness. Among the transition elements tested (Fe^{2+}, Ni^{2+}, Cu^{2+}, and Ag^{+}), only silver and iron caused E110 decolorization without the need for thermal activation. This finding may be explained by their ability to initiate the PS activation process. The decolorization's observed thermodynamic parameters (E_a, $\Delta H^{\neq}$, $\Delta S^{\neq}$ and $\Delta G^{\neq}$) were calculated using the observed rates obtained at various temperatures. Finally, the destruction of aromatic ring structures accompanies the discoloration of E110.

*Author Information**

*The authors' names are presented in the following order: First Name, Middle Name and Last Name

Nedjma Lahmar — Student in Environmental Chemistry, Inorganic Materials Laboratory, University of M'sila, University Pole, Road Bourdj Bou Arreiridj, 28000, M'sila Algeria; *e-mail*: nedjma.lahmar@univ-msila.dz; https://orcid.org/0009-0005-1849-0751

Mokhtar Djehiche (*corresponding author*) — Doctor of Atmospheric Chemistry, Inorganic Materials Laboratory, University of M'sila, University Pole, Road Bourdj Bou Arreiridj, 28000, M'sila Algeria; *e-mail*: mokhtar.djehiche@univ-msila.dz; https://orcid.org/0000-0002-3439-113X

Marwa Bachiri — Student in Environmental Chemistry, Inorganic Materials Laboratory, University of M'sila, University Pole, Road Bourdj Bou Arreiridj, 28000, M'sila Algeria; *e-mail*: marwa.bachiri@univ-msila.dz; https://orcid.org/0009-0006-1133-5801

Author Contributions

The manuscript was written through contributions of all authors. All authors have given approval to the final version of the manuscript. CRediT: **Nedjma Lahmar** conceptualization, investigation, methodology, validation, visualization, writing — original draft; **Mokhtar Djehiche** Supervision, formal analysis, visualization, writing — review & editing; **Marwa Bachiri** investigation.

Acknowledgments

The authors thank the University of Mohamed Boudiaf for access to the library facilities.

Conflicts of Interest

The authors declare no conflict of interest.

References

1 Rajamanickam, D., Shanthi, M. (2014). Photocatalytic degradation of an azo dye Sunset Yellow under UV-A light using TiO_2/CAC composite catalysts. *Spectrochim Acta A Mol Biomol Spectrosc, 128*, 100–108. https://doi.org/10.1016/j.saa.2014.02.126

2 Amchova, P., Kotolova, H., Ruda-Kucerova, J. (2015). Health safety issues of synthetic food colorants. *Regul Toxicol Pharmacol, 73*, 914–922. https://doi.org/10.1016/j.yrtph.2015.09.026

3 Rovina, K., Prabakaran, P.P., Siddiquee, S., Shaarani, S.M. (2016). Methods for the analysis of Sunset Yellow FCF (E110) in food and beverage products- a review. *TrAC Trends Anal Chem, 85*, 47–56. https://doi.org/10.1016/j.trac.2016.05.009

4 Chen, H. (2012). Toxicological significance of azo dye metabolism by human intestinal microbiota. *Front Biosci, E4*, 568–586. https://doi.org/10.2741/e400

5 Levine, W.G. (1991). Metabolism of AZO Dyes: Implication for Detoxication and Activation. *Drug Metab Rev, 23*, 253–309. https://doi.org/10.3109/03602539109029761

6 Hashemi, S.H., Kaykhaii, M. (2022). Azo dyes: Sources, occurrence, toxicity, sampling, analysis, and their removal methods. In: *Emerging Freshwater Pollutants*, 267–287. Elsevier.

7 Fatimah, A. (2020). Role of microorganisms in biodegradation of food additive Azo dyes: A review. *Afr J Biotechnol, 19*, 799–805. https://doi.org/10.5897/AJB2020.17250

8 Minioti, K.S., Sakellariou, C.F., Thomaidis, N.S. (2007). Determination of 13 synthetic food colorants in water-soluble foods by reversed-phase high-performance liquid chromatography coupled with diode-array detector. *Anal Chim Acta, 583*, 103–110. https://doi.org/10.1016/j.aca.2006.10.002

9 Sha, O., Zhu, X., Feng, Y., Ma, W. (2015). Aqueous two-phase based on ionic liquid liquid–liquid microextraction for simultaneous determination of five synthetic food colourants in different food samples by high-performance liquid chromatography. *Food Chem, 174*, 380–386. https://doi.org/10.1016/j.foodchem.2014.11.068

10 Newsome, A.G., Culver, C.A., Van Breemen, R.B. (2014). Nature's Palette: The Search for Natural Blue Colorants. *J Agric Food Chem, 62*, 6498–6511. https://doi.org/10.1021/jf501419q

11 Axon, A., May, F.E.B., Gaughan, L.E., et al. (2012). Tartrazine and sunset yellow are xenoestrogens in a new screening assay to identify modulators of human oestrogen receptor transcriptional activity. *Toxicology, 298*, 40–51. https://doi.org/10.1016/j.tox.2012.04.014

12 Sarıkaya, R., Selvi, M., Erkoç, F. (2012). Evaluation of potential genotoxicity of five food dyes using the somatic mutation and recombination test. *Chemosphere, 88*, 974–979. https://doi.org/10.1016/j.chemosphere.2012.03.032

13 Ma, J., Li, H., Chi, L., et al. (2017). Changes in activation energy and kinetics of heat-activated persulfate oxidation of phenol in response to changes in pH and temperature. *Chemosphere, 189*, 86–93. https://doi.org/10.1016/j.chemosphere.2017.09.051

14 Wacławek, S., Lutze, H.V., Grübel, K., et al. (2017). Chemistry of persulfates in water and wastewater treatment: A review. *Chem Eng J, 330*, 44–62. https://doi.org/10.1016/j.cej.2017.07.132

15 Ahmadi, S., Igwegbe, C.A., Rahdar, S. (2019). The application of thermally activated persulfate for degradation of Acid Blue 92 in aqueous solution. *Int J Ind Chem, 10*, 249–260. https://doi.org/10.1007/s40090-019-0188-1

16 Bing, W., Wei, W. (2019). Degradation Phenol Wastewater by Heating Activated Persulfate. *Int J Environ Monit Anal, 7*, 14. https://doi.org/10.11648/j.ijema.20190701.12

17 Wang, Z., Qiu, W., Pang, S., et al. (2020). Relative contribution of ferryl ion species (Fe(IV)) and sulfate radical formed in nanoscale zero valent iron activated peroxydisulfate and peroxymonosulfate processes. *Water Res, 172*, 115504. https://doi.org/10.1016/j.watres.2020.115504

18 Dong, H., He, Q., Zeng, G., et al. (2017). Degradation of trichloroethene by nanoscale zero-valent iron (nZVI) and nZVI activated persulfate in the absence and presence of EDTA. *Chem Eng J, 316*, 410–418. https://doi.org/10.1016/j.cej.2017.01.118

19 Hou, S., Ling, L., Shang, C., et al. (2017). Degradation kinetics and pathways of haloacetonitriles by the UV/persulfate process. *Chem Eng J, 320*, 478–484. https://doi.org/10.1016/j.cej.2017.03.042

20 Miao, D., Zhao, S., Zhu, K., et al. (2020). Activation of persulfate and removal of ethyl-parathion from soil: Effect of microwave irradiation. *Chemosphere, 253*, 126679. https://doi.org/10.1016/j.chemosphere.2020.126679

21 Gao, Y., Gao, N., Wang, W., et al. (2018). Ultrasound-assisted heterogeneous activation of persulfate by nano zero-valent iron (nZVI) for the propranolol degradation in water. *Ultrason Sonochem, 49*, 33–40. https://doi.org/10.1016/j.ultsonch.2018.07.001

22 Matzek, L.W., Tipton, M.J., Farmer, A.T., et al. (2018). Understanding Electrochemically Activated Persulfate and Its Application to Ciprofloxacin Abatement. *Environ Sci Technol, 52*, 5875–5883. https://doi.org/10.1021/acs.est.8b00015

23 Bhatia, S.C. (2014). Solar thermal energy. In: Advanced Renewable Energy Systems. Elsevier, 94–143.

24 Jakubauskaite, V., Dikun, J., Jankunas, V., et al. (2015). Use of solar water heating system for oil contaminated soil treatment. In: 2015 Tenth International Conference on Ecological Vehicles and Renewable Energies (EVER). IEEE, Monte Carlo, 1–10.

25 Liang, C., Su, H.-W. (2009). Identification of Sulfate and Hydroxyl Radicals in Thermally Activated Persulfate. *Ind Eng Chem Res, 48*, 5558–5562. https://doi.org/10.1021/ie9002848

26 House, D.A. (1962). Kinetics and Mechanism of Oxidations by Peroxydisulfate. *Chem Rev, 62*, 185–203. https://doi.org/10.1021/cr60217a001

27 Sun, S.-P., Li, C.-J., Sun, J.-H., et al. (2009). Decolorization of an azo dye Orange G in aqueous solution by Fenton oxidation process: Effect of system parameters and kinetic study. *J Hazard Mater, 161*, 1052–1057. https://doi.org/10.1016/j.jhazmat.2008.04.080

28 Riga, A., Soutsas, K., Ntampegliotis, K., et al. (2007). Effect of system parameters and of inorganic salts on the decolorization and degradation of Procion H-exl dyes. Comparison of H_2O_2/UV, Fenton, UV/Fenton, TiO_2/UV and TiO_2/UV/H_2O_2 processes. *Desalination, 211*, 72–86. https://doi.org/10.1016/j.desal.2006.04.082

29 Bennedsen, L.R., Muff, J., Søgaard, E.G. (2012). Influence of chloride and carbonates on the reactivity of activated persulfate. *Chemosphere, 86*, 1092–1097. https://doi.org/10.1016/j.chemosphere.2011.12.011

30 Liang, C.-J., Huang, S.-C. (2012). Kinetic model for sulfate/hydroxyl radical oxidation of methylene blue in a thermally-activated persulfate system at various pH and temperatures. *Sustain Env Res*, 199–208.

31 Wei, L., Xia, X., Zhu, F., et al. (2020). Dewatering efficiency of sewage sludge during Fe^{2+}-activated persulfate oxidation: Effect of hydrophobic/hydrophilic properties of sludge EPS. *Water Res, 181*, 115903. https://doi.org/10.1016/j.watres.2020.115903

32 Baciocchi, R., D'Aprile, L., Innocenti, I., et al. (2014). Development of technical guidelines for the application of in-situ chemical oxidation to groundwater remediation. *J Clean Prod, 77*, 47–55. https://doi.org/10.1016/j.jclepro.2013.12.016

33 Matzek, L.W., Carter, K.E. (2016). Activated persulfate for organic chemical degradation: A review. *Chemosphere, 151*, 178–188. https://doi.org/10.1016/j.chemosphere.2016.02.055

34 Oranusi, N., Njoku, H. (2009). Biotransformation of Food Dyes by Human Intestinal Bacteria (Streptococcus faecalis, Eschericia coli). *J Appl Sci Environ Manag, 10*. https://doi.org/10.4314/jasem.v10i2.43698

35 Abdel-Aziz, H.M., Abdel-Gawad, S.A. (2020). Removal of sunset YellowAzo dye using activated carbon entrapped in alginate from aqueous solutions. *Open Access J Sci, 4*, 1–6. https://doi.org/10.15406/oajs.2020.04.00142

36 Feizi, R., Ahmad, M., Jorfi, S., Ghanbari, F. (2019). Sunset yellow degradation by ultrasound/peroxymonosulfate/$CuFe_2O_4$: Influential factors and degradation processes. *Korean J Chem Eng, 36*, 886–893. https://doi.org/10.1007/s11814-019-0268-0

37 Shuchi, S.B., Suhan, Md.B.K., Humayun, S.B., et al. (2021). Heat-activated potassium persulfate treatment of Sudan Black B dye: Degradation kinetic and thermodynamic studies. *J Water Process Eng, 39*, 101690. https://doi.org/10.1016/j.jwpe.2020.101690

38 Wang, S., Zhou, N. (2016). Removal of carbamazepine from aqueous solution using sono-activated persulfate process. *Ultrason Sonochem, 29*, 156–162. https://doi.org/10.1016/j.ultsonch.2015.09.008

39 Fayoumi, L.M.A., Ezzedine, M.A., Akel, H.H., Jamal, M.M. (2012). Kinetic Study of the Degradation of Crystal Violet by $K_2S_2O_8$. Comparison with Malachite Green: *Port Electrochimica Acta, 30*, 121–133. https://doi.org/10.4152/pea.201202121

40 Naser Elddine, H.A., Damaj, Z.K., Yazbeck, O.A., et al. (2015). Kinetic Study of the Discoloration of the Food Colorant E131 by $K_2S_2O_8$ and KIO_3: *Port Electrochimica Acta, 33*, 275–288. https://doi.org/10.4152/pea.201505275

41 Lian, L., Yao, B., Hou, S., et al. (2017). Kinetic Study of Hydroxyl and Sulfate Radical-Mediated Oxidation of Pharmaceuticals in Wastewater Effluents. *Environ Sci Technol, 51*, 2954–2962. https://doi.org/10.1021/acs.est.6b05536

42 Ahmadi, M., Behin, J., Mahnam, A.R. (2016). Kinetics and thermodynamics of peroxydisulfate oxidation of Reactive Yellow 84. *J Saudi Chem Soc, 20*, 644–650. https://doi.org/10.1016/j.jscs.2013.07.004

43 Mora, V.C., Rosso, J.A., Carrillo Le Roux, G., et al. (2009). Thermally activated peroxydisulfate in the presence of additives: A clean method for the degradation of pollutants. *Chemosphere, 75*, 1405–1409. https://doi.org/10.1016/j.chemosphere.2009.02.038

44 Chen, L., Xue, Y., Luo, T., et al. (2021). Electrolysis-assisted UV/sulfite oxidation for water treatment with automatic adjustments of solution pH and dissolved oxygen. *Chem Eng J, 403*, 126278. https://doi.org/10.1016/j.cej.2020.126278

45 Djehiche, M., Tomas, A., Fittschen, C., Coddeville, P. (2011). First Direct Detection of HONO in the Reaction of Methylnitrite (CH_3ONO) with OH Radicals. *Environ Sci Technol, 45*, 608–614. https://doi.org/10.1021/es103076e

46 Djehiche, M., Tomas, A., Fittschen, C., Coddeville, P. (2011). First Cavity Ring-Down Spectroscopy HO_2 Measurements in a Large Photoreactor. *Z Für Phys Chem, 225*, 938–992. https://doi.org/10.1524/zpch.2011.0143

47 Johnson, R.L., Tratnyek, P.G., Johnson, R.O. (2008). Persulfate Persistence under Thermal Activation Conditions. *Environ Sci Technol, 42*, 9350–9356. https://doi.org/10.1021/es8019462

48 Yu, X.-Y., Bao, Z.-C., Barker, J.R. (2004). Free Radical Reactions Involving $Cl^{\bullet}$, $Cl_2^{-\bullet}$, and $SO_4^{-\bullet}$ in the 248 nm Photolysis of Aqueous Solutions Containing $S_2O_8^{2-}$ and Cl^-. *J Phys Chem A, 108*, 295–308. https://doi.org/10.1021/jp036211i

49 Hayon, E., McGarvey, J.J. (1967). Flash photolysis in the vacuum ultraviolet region of sulfate, carbonate, and hydroxyl ions in aqueous solutions. *J Phys Chem, 71*, 1472–1477. https://doi.org/10.1021/j100864a044

50 Wojnárovits, L., Takács, E. (2019). Rate constants of sulfate radical anion reactions with organic molecules: A review. *Chemosphere, 220*, 1014–1032. https://doi.org/10.1016/j.chemosphere.2018.12.156

51 Yang, B., Luo, Q., Li, Q., et al. (2021). Selective oxidation and direct decolorization of cationic dyes by persulfate without activation. *Water Sci Technol, 83*, 2744–2752. https://doi.org/10.2166/wst.2021.177

52 Mcheik, A.H., Jamal, M.M.E. (2013). Kinetic Study of the Discoloration of Rhodamine B with Persulfate, Iron Activation. *J Chem Technol Metall*, 357–365.

53 Ji, Y., Wang, L., Jiang, M., et al. (2017). The role of nitrite in sulfate radical-based degradation of phenolic compounds: An unexpected nitration process relevant to groundwater remediation by in-situ chemical oxidation (ISCO). *Water Res, 123*, 249–257. https://doi.org/10.1016/j.watres.2017.06.081

54 Yang, P., Ji, Y., Lu, J., Huang, Q. (2019). Formation of Nitrophenolic Byproducts during Heat-Activated Peroxydisulfate Oxidation in the Presence of Natural Organic Matter and Nitrite. *Environ Sci Technol, 53*, 4255–4264. https://doi.org/10.1021/acs.est.8b06967

55 Shannon, R.D. (1976) Revised effective ionic radii and systematic studies of interatomic distances in halides and chalcogenides. *Acta Crystallogr Sect A, 32*, 751–767. https://doi.org/10.1107/S0567739476001551

56 Zhangm, H.-C., Han, J.-J., Zhang, X., et al. (2021). Undiscovered Multiple Roles of Multivalent Cations in the Pollutant Removal from Actual Water by Persulfate Activated by Carbon Materials. *ACS EST Eng, 1*, 1227–1235. https://doi.org/10.1021/acsestengg.1c00121

57 Zhang, R., Wang, X., Zhou L, Crump D (2019). Quantum chemical investigations of the decomposition of the peroxydisulfate ion to sulfate radicals. *Chem Eng J, 361*, 960–967. https://doi.org/10.1016/j.cej.2018.12.145

58 Xia, X., Zhu, F., Li, J., et al. (2020). A Review Study on Sulfate-Radical-Based Advanced Oxidation Processes for Domestic/Industrial Wastewater Treatment: Degradation, Efficiency, and Mechanism. *Front Chem, 8*, 592056. https://doi.org/10.3389/fchem.2020.592056

59 Park, S.-M., Lee, S.-W., Jeon, P.-Y., Baek, K. (2016). Iron Anode-Mediated Activation of Persulfate. *Water Air Soil Pollut, 227*, 462. https://doi.org/10.1007/s11270-016-3169-4

60 Anipsitakis, G.P., Dionysiou, D.D. (2004). Radical Generation by the Interaction of Transition Metals with Common Oxidants. *Environ Sci Technol, 38*, 3705–3712. https://doi.org/10.1021/es035121o

61 Bing, W., Wei, W. (2019). Degradation Phenol Wastewater by Heating Activated Persulfate. *Int J Environ Monit Anal, 7*, 14. https://doi.org/10.11648/j.ijema.20190701.12

62 Criquet, J., Leitner, N.K.V. (2009). Degradation of acetic acid with sulfate radical generated by persulfate ions photolysis. *Chemosphere, 77*, 194–200. https://doi.org/10.1016/j.chemosphere.2009.07.040

63 Thabet, M., El-Zomrawy, A.A. (2016). Degradation of acid red 17 dye with ammonium persulphate in acidic solution using photoelectrocatalytic methods. *Arab J Chem, 9*, S204–S208. https://doi.org/10.1016/j.arabjc.2011.03.001

64 Wang, C., Yang, Q., Li, Z., et al. (2019). A novel carbon-coated Fe-C/N composite as a highly active heterogeneous catalyst for the degradation of Acid Red 73 by persulfate. *Sep Purif Technol, 213*, 447–455. https://doi.org/10.1016/j.seppur.2018.12.072

65 Ghauch, A., Tuqan, A.M., Kibbi, N., Geryes, S. (2012). Methylene blue discoloration by heated persulfate in aqueous solution. *Chem Eng J, 213*, 259–271. https://doi.org/10.1016/j.cej.2012.09.122

66 Lee, Y.-C., Lo, S.-L., Kuo, J., Lin, Y.-L. (2012). Persulfate oxidation of perfluorooctanoic acid under the temperatures of 20–40 °C. *Chem Eng J, 198–199*, 27–32. https://doi.org/10.1016/j.cej.2012.05.073

67 Furman, O.S., Teel, A.L., Ahmad, M., et al. (2011). Effect of Basicity on Persulfate Reactivity. *J Environ Eng, 137*, 241–247. https://doi.org/10.1061/(ASCE)EE.1943-7870.0000323

68 Liang, C., Wang, Z.-S., Bruell, C.J. (2007). Influence of pH on persulfate oxidation of TCE at ambient temperatures. *Chemosphere, 66*, 106–113. https://doi.org/10.1016/j.chemosphere.2006.05.026

69 Chmiel, H., Kaschek, M., Blöcher, C., et al. (2003). Concepts for the treatment of spent process water in the food and beverage industries. *Desalination, 152*, 307–314. https://doi.org/10.1016/S0011-9164(02)01078-0

70 Suzuki, M., Suzuki, Y., Uzuka, K., Kawase, Y. (2020). Biological treatment of non-biodegradable azo-dye enhanced by zero-valent iron (ZVI) pre-treatment. *Chemosphere, 259*, 127470. https://doi.org/10.1016/j.chemosphere.2020.127470

71 Feuzer-Matos, A.J., Testolin, R.C., Pimentel-Almeida, W., et al. (2022). Treatment of Wastewater Containing New and Non-biodegradable Textile Dyes: Efficacy of Combined Advanced Oxidation and Adsorption Processes. *Water Air Soil Pollut, 233*, 273. https://doi.org/10.1007/s11270-022-05751-1

72 Rahmani, A.R., Rezaeivahidian, H., Almasi, M., et al. (2016). A comparative study on the removal of phenol from aqueous solutions by electro–Fenton and electro–persulfate processes using iron electrodes. *Res Chem Intermed, 42*, 1441–1450. https://doi.org/10.1007/s11164-015-2095-1

73 Luo, Q. (2014). Oxidative treatment of aqueous monochlorobenzene with thermally-activated persulfate. *Front Environ Sci Eng, 8*, 188–194. https://doi.org/10.1007/s11783-013-0544-x

74 Fragoso, C.T., Battisti, R., Miranda, C., De Jesus, P.C. (2009). Kinetic of the degradation of C.I. Food Yellow 3 and C.I. Food Yellow 4 azo dyes by the oxidation with hydrogen peroxide. *J Mol Catal Chem, 301*, 93–97. https://doi.org/10.1016/j.molcata.2008.11.014

75 Xu, X.-R., Li, X.-Z. (2010). Degradation of azo dye Orange G in aqueous solutions by persulfate with ferrous ion. *Sep Purif Technol, 72*, 105–111. https://doi.org/10.1016/j.seppur.2010.01.012

76 Hu, E., Wu, X., Shang, S., et al. (2016). Catalytic ozonation of simulated textile dyeing wastewater using mesoporous carbon aerogel supported copper oxide catalyst. *J Clean Prod, 112*, 4710–4718. https://doi.org/10.1016/j.jclepro.2015.06.127

77 Wu, C.-H., Kuo, C.-Y., Chang, C.-L. (2008). Homogeneous catalytic ozonation of C.I. Reactive Red 2 by metallic ions in a bubble column reactor. *J Hazard Mater, 154*, 748–755. https://doi.org/10.1016/j.jhazmat.2007.10.087

78 Hori, H., Yamamoto, A., Hayakawa, E., et al. (2005). Efficient Decomposition of Environmentally Persistent Perfluorocarboxylic Acids by Use of Persulfate as a Photochemical Oxidant. *Environ Sci Technol, 39*, 2383–2388. https://doi.org/10.1021/es0484754

79 Anipsitakis, G.P., Dionysiou, D.D., Gonzalez, M.A. (2006). Cobalt-Mediated Activation of Peroxymonosulfate and Sulfate Radical Attack on Phenolic Compounds. Implications of Chloride Ions. *Environ Sci Technol, 40*, 1000–1007. https://doi.org/10.1021/es050634b

80 Gokulakrishnan, S., Parakh, P., Prakash, H. (2012). Degradation of Malachite green by Potassium persulphate, its enhancement by 1,8-dimethyl-1,3,6,8,10,13-hexaazacyclotetradecane nickel(II) perchlorate complex, and removal of antibacterial activity. *J Hazard Mater, 213-214*, 19–27. https://doi.org/10.1016/j.jhazmat.2012.01.031